Biophysical Journal

Supporting Material

A Force Balance Explains Local and Global Cell Movements during Early Zebrafish Development

Jack Chai,[1] Andrea L. Hamilton,[2] Michael Krieg,[2] Craig D. Buckley,[1] Ingmar H. Riedel-Kruse,[3] and Alexander R. Dunn[1,4,*]

[1]Dept. of Chemical Engineering, Stanford University, [2]Dept. of Molecular and Cellular Physiology, Stanford School of Medicine, [3]Dept. of Bioengineering, Stanford University, and [4]Stanford Cardiovascular Institute, Stanford University School of Medicine, Stanford, California 94305

3D modeling on an ellipsoid

General description of 3D modeling of epiboly

For the 3D model, we assume the same two forces as we did in the 2D model: F_{Tan}, the driving force of epiboly directed along the surface of the embryo, and F_{CCT}, the cable constriction tension generated by the actin band that is directed towards the center of the actin band. In the sections below, we describe how F_{Tan} and F_{CCT} may be reasonably defined, and how we defined these quantities in our analytical model and simulations.

Description of F_{Tan}

F_{Tan} is defined along the surface of the embryo since all the processes of epiboly including microtubule polymerization and flow friction occur on the surface of the embryo. (1-7) We employ the simplifying assumptions the forces generated in F_{Tan} are uniform along each point of the margin and depends only on the current configuration of the embryo since, as shown below, more complex alternatives are not required to explain our observations.

Description of F_{CCT}

Prior evidence (2, 8, 9) suggests that the actin band exerts a line tension at the blastoderm margin that results in an inward-pointing force termed $F_{CCT.}$ Multiple methods exist for modeling line tensions. One such possibility would be to represent the line tension by springs along the margin of the blastoderm. Another such possibility would be to scale the tension along the margin as inversely proportional to the local radius of curvature (Force is proportional to 1/r), similar to the pressure difference generated in a Young-Laplace law. In both models, the areas of highest curvature have the greatest force that is pointed towards the center of the ring: in the case of the springs, the springs are oriented more towards the center, and in the curvature example, the areas of lowest curvature are along the major axis (Figure S5). A consequence of these models is that the force is highest along the major axis and lowest along the minor axis and adopts intermediate force values in between these two points. In the sections below, we scale F_{CCT} by the distance of the point along the margin to the center of the band, which results in a similar results as the spring and curvature models. This approximation results in a tractable, analytical solution.

Setting the geometry of the embryo

In order to understand the effects of geometry on the actin band in 3D, we began by modeling the embryo as an ellipsoid centered at (0,0,0) in Cartesian coordinates:

$$\frac{x^2}{a^2}+\frac{y^2}{b^2}+\frac{z^2}{c^2}=1 \quad \text{(S1)}$$

We will first solve the general case in which a, b and c are not equal. Later, we will show that the case in which $a = b$ results in a simple linear solution. We designate the z-axis as the long axis such that $c > a$ and $c > b$. Without loss of generality, we specify that the animal pole corresponds to a positive z-value.

We begin on this ellipsoid by defining the ring for the actin band, which can be expressed by intersecting a plane with the ellipsoid described in equation S1 (Figure S4A). If we make the yz-plane the equivalent of our experimental observation plane, we can assume that the ring will be symmetric with respect to the yz-plane. Consequently, we can define the intersection plane to be:

$$z = my + d \quad \text{(S2)}$$

The slope m defines the angle of the ring, such that any non-zero value creates an intersection plane that is asymmetric with respect to the ellipsoid. The intercept d represents the progress of epiboly. At the start of epiboly the ring is located more towards the animal pole and the intercept d has a positive value. As epiboly progresses d decreases. We obtain an equation for the ring by combining equations S1 and S2:

$$\frac{x^2}{a^2}+\frac{y^2}{b^2}+\frac{(my+d)^2}{c^2}=1 \quad \text{(S3)}$$

Defining F_{CCT}

As described in the in the sections above, F_{CCT} points toward the center of the ring and is scaled by the distance from the center of the ring. To find the center of the ring we note that we have defined the ring symmetric as with respect to the yz-plane. Consequently, the center of the ring must be located at $x = 0$. Solving the set of equations in (S2) and (S3) when x = 0, we observe that the center of the ring (x',y',z') is located at:

$$x' = 0$$
$$y' = \frac{-mdb^2}{c^2 + m^2 b^2} \tag{S4}$$
$$z' = \frac{dc^2}{c^2 + m^2 b^2}$$

We can confirm that our solution for the ring center is correct through the following observations. When $m = 0$ we expect that the ring to be parallel to the xy plane centered along the z-axis (Figure S4B). When $d = 0$, we expect the ring to cut through the center of the ellipsoid. (Figure S4C).

We define the normalized vector for F_{CCT} at any arbitrary point (x_1, y_1, z_1) on the ring:

$$F_{CCT,x,norm} = \frac{-(x_1 - x')}{\left\| F_{CCT,norm} \right\|} \tag{S5a}$$

$$F_{CCT,y,norm} = \frac{-(y_1 - y')}{\left\| F_{CCT,norm} \right\|} \tag{S5b}$$

$$F_{CCT,z,norm} = \frac{-(z_1 - z')}{\left\| F_{CCT,norm} \right\|} \tag{S5c}$$

||CCT|| is a normalization factor that is defined as shown:

$$\left\| F_{CCT,norm} \right\| = \frac{2\int \sqrt{(F_{CCT,x,norm}{}^2 + F_{CCT,y,norm}{}^2 + F_{CCT,z,norm}{}^2)}\, dy_1}{2\int dy_1} \tag{S6}$$

The integral is a line integral around the entire ring. The factor of 2 in both the numerator and denominator reflect the fact that each y_1 value has two corresponding x_1 value. Since the shape we are using is symmetric across the *yz*-plane, the positive and negative x_1 arcs have equal integrals. Consequently, the integral around the entire ring can be obtained by doubling the integral on an arc of a positive x_1 ring. Also, note that $||F_{CCT,norm}||$ is constant. The normalized vectors, as defined here, do not have magnitudes equal to 1, but instead maintain the scaling as defined by the distance to the ring center.

Defining F_{Tan}

Simple geometric observations show that the tangent vector must lie on two distinct planes. First, the tangent vector must exist on a surface tangent at the point on the ring (x_1, y_1, z_1; Figure S4D). A tangent to the surface at this point can be found by finding the plane perpendicular to the surface normal as shown by defining a function:

$$f(x,y,z) = 1 - \frac{x^2}{a^2} + \frac{y^2}{b^2} + \frac{z^2}{c^2} \tag{S8}$$

The surface normal is given by the gradient of *f* following a derivative of S8:

$$\vec{n}(x_1,y_1,z_1) = \nabla f\big|_{x_1,y_1,z_1} = \left(\frac{2x_1}{a^2}, \frac{2y_1}{b^2}, \frac{2z_1}{c^2}\right) \tag{S9}$$

The surface normal is a vector which is by definition perpendicular to the surface of the ellipsoid. Since we know that F_{Tan} lies on the surface of the ellipsoid, we can find the plane that is perpendicular to the surface normal to find the plane on which F_{Tan} must lie. At the point (x_1,y_1,z_1), this will generate the following equations for the tangent plane to the surface derived by taking find the perpendicular plane to equation S9:

$$\begin{aligned} &\vec{n}(x_1,y_1,z_1) \bullet (x-x_1, y-y_1, z-z_1) = 0 \\ &\frac{2x_1}{a^2}(x-x_1) + \frac{2y_1}{b^2}(y-y_1) + \frac{2z_1}{c^2}(z-z_1) = 0 \end{aligned} \tag{S10}$$

Second, the tangent vector corresponding to F_{Tan} must also exist on the plane that contains the point on the ring, (x_1,y_1,z_1); the center of the ring, (x',y',z'); and the center of the ellipsoid, (0,0,0) (Figure S4D). This follows from the choice of coordinates: the center of the ring necessarily passes through (0,0,0) due to the initial choice of the *yz* plane. The plane determined by these three points can be defined as below:

$$\begin{vmatrix} x-0 & y-0 & z-0 \\ x'-0 & y'-0 & z'-0 \\ x_1-0 & y_1-0 & z_1-0 \end{vmatrix} = 0$$

$$x(y'z_1 - y_1z') - y(x'z_1 - x_1z') + z(x'y_1 - x_1y') = 0 \tag{S11}$$

When we solve equations S10 and S11 simultaneously, we obtain

$$\alpha y - \beta z + \gamma = 0 \tag{S12}$$

Where

$$\alpha = \left(\frac{2x_1^2 z'}{a^2} - \frac{2y_1(y'z_1 - y_1z')}{b^2} \right) = \frac{2d(c^2 - d^2)}{c^2 + m^2b^2} \tag{S13}$$

$$\beta = \left(\frac{2x_1^2 y'}{a^2} + \frac{2z_1(y'z_1 - y_1z')}{c^2} \right) = \frac{-2d(mb^2 + dy_1)}{c^2 + m^2b^2} \tag{S14}$$

$$\gamma = \frac{2x_1^2}{a^2} y'z_1 - \frac{2x_1^2}{a^2} y_1z' + \left(\frac{2y_1^2}{b^2} + \frac{2z_1^2}{c^2} \right)(y'z_1 - y_1z') \tag{S15}$$

According to the definition of the coordinate system, movement along the tangent vectors will result in a negative progression along the *z*-axis. Consequently, for locations other than the poles, we differentiate with respect to negative movement in *z* to obtain the normalized tangent vectors. By differentiating equation S12 with respect to negative movement in *z*, we can obtain

the *y*-component of the tangent. Similarly, differentiating equation S10 yields the *x*-component of the tangent:

$$F_{Tan,x,norm} = \frac{-\frac{x_1\left(y' - z'\frac{\beta}{\alpha}\right)}{y'z_1 - y_1z'}}{\left\|F_{Tan,norm}\right\|} = \frac{\frac{x_1(md^3b^2 + d^2c^2y_1)}{(c^2 - d^2)(m^2db^2y_1 + md^2b^2 + dy_1c^2)}}{\left\|F_{Tan,norm}\right\|} \quad \text{(S16a)}$$

$$F_{Tan,y,norm} = \frac{-\left(\frac{\beta}{\alpha}\right)}{\left\|F_{Tan,norm}\right\|} = \frac{\frac{mb^2 + dy_1}{c^2 - d^2}}{\left\|F_{Tan,norm}\right\|} \quad \text{(S16b)}$$

$$F_{Tan,z,norm} = \frac{-1}{\left\|F_{Tan,norm}\right\|} \quad \text{(S16c)}$$

In this form, $F_{Tan,norm}$ is defined to normalize the vector to unity and can be calculated by:

$$\left\|F_{Tan,norm}\right\| = \sqrt{\left(\frac{x_1\left(y' - z'\frac{\beta}{\alpha}\right)}{y'z_1 - y_1z'}\right)^2 + \left(\frac{\beta}{\alpha}\right)^2 + (-1)^2} \quad \text{(S17)}$$

Simulating epiboly progression

Having obtained all components of the tangent vector and the CCT vector, we can find the angle θ as a function of position on the ring:

$$\cos(\theta) = \vec{F}_{CCT,norm} \bullet \vec{F}_{Tan,norm} = \frac{-\frac{a^2\beta}{b^2\alpha}y_1 + \frac{\beta}{\alpha}y_1 + \left(\frac{mdb^2}{c^2 + m^2b^2}\right)\frac{\beta}{\alpha} - \frac{a^2}{c^2}z_1 + z_1 - \frac{dc^2}{c^2 + m^2b^2}}{\left\|F_{Tan,norm}\right\|\left\|F_{CCT,norm}\right\|} \quad \text{(S18a)}$$

If we assume symmetry around the *z*-axis ($a = b$) and substitute in Equation S2 we obtain:

$$\cos(\theta) = \vec{F}_{CCT,norm} \bullet \vec{F}_{Tan,norm} = \frac{\left(\frac{mdb^2}{c^2 + m^2 b^2}\right)\left(\frac{mb^2 + dy_1}{c^2 - d^2}\right) + \left(1 - \frac{b^2}{c^2}\right)(my_1 + d) - \frac{dc^2}{c^2 + m^2 b^2}}{\left\|F_{Tan,norm}\right\|\left\|F_{CCT,norm}\right\|} \quad \text{(S18b)}$$

From this we observe that the correlation between the CCT and tangent vectors are linear with respect to movement in *y* in the *yz*-plane, which is consistent with our presentation of the 2D model. If we model embryo development using experimentally determined values of F_{CCT} and F_{Tan} (Figure S4E-G), we see that in a spherical embryo ($a = b = c$), the migration pattern of this ring is uniform around the sphere (Figure S4E and Movie S2). If the initial blastoderm mass is symmetric with respect to the z-axis ($m = 0$) the blastoderm likewise migrates uniformly, as would be expected (Figure S4F and Movie S3). However, if we place the initial ring in an asymmetric location, the blastoderm migrates unevenly and rotates to be symmetric along the long axis, as was observed experimentally (Figure S4G and Movie S4).

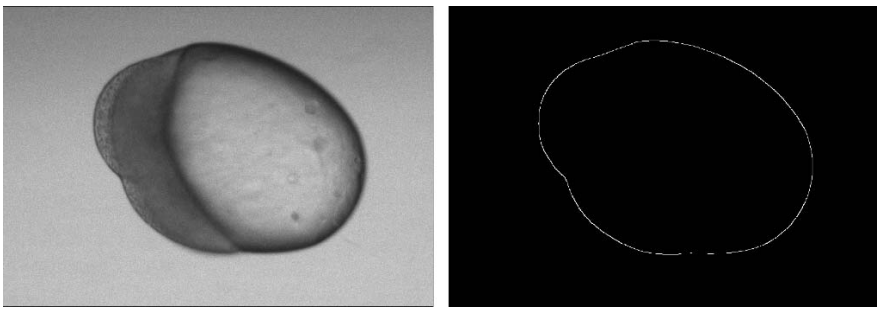

Figure S1: *Left:* Image of a compressed zebrafish embryo. Right: boundary determination using a Canny-Deriche edge detection algorithm.

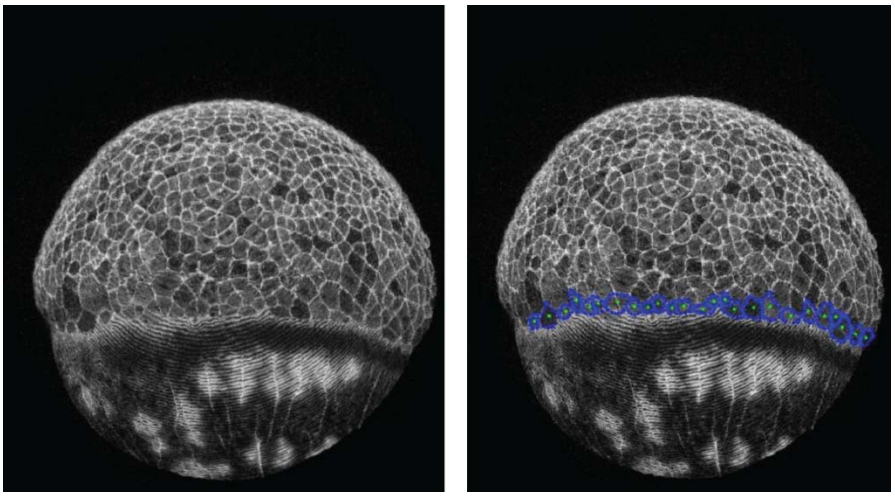

Figure S2: Quantification of cell-cell correlation at the blastoderm margin in a uncompressed embryo grown in normal E2 media. *Left*: Image of a TMR-phalloidin stained embryo. *Right*: The outlines of the cells at the margin were determined manually. Blue outlines show the cell boundary. The green dots indicate the calculated center of the cell.

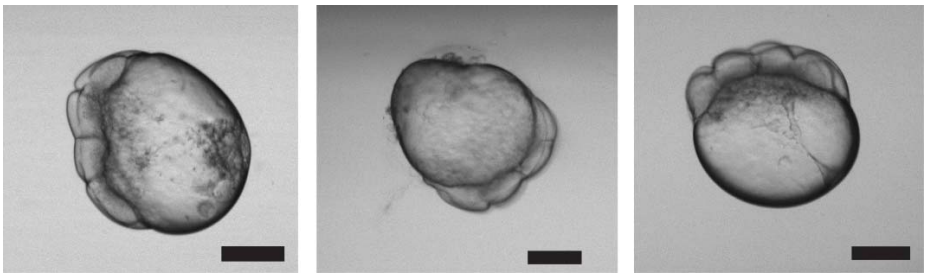

Figure S3: Examples of different shapes adopted by embryos under agar compression. Compression can induce highly asymmetrical shapes as seen in the left and middle panels. Compression can also induce minor deviations from axial symmetry without an apparent long axis (right panel). Scale bar = 250 μm.

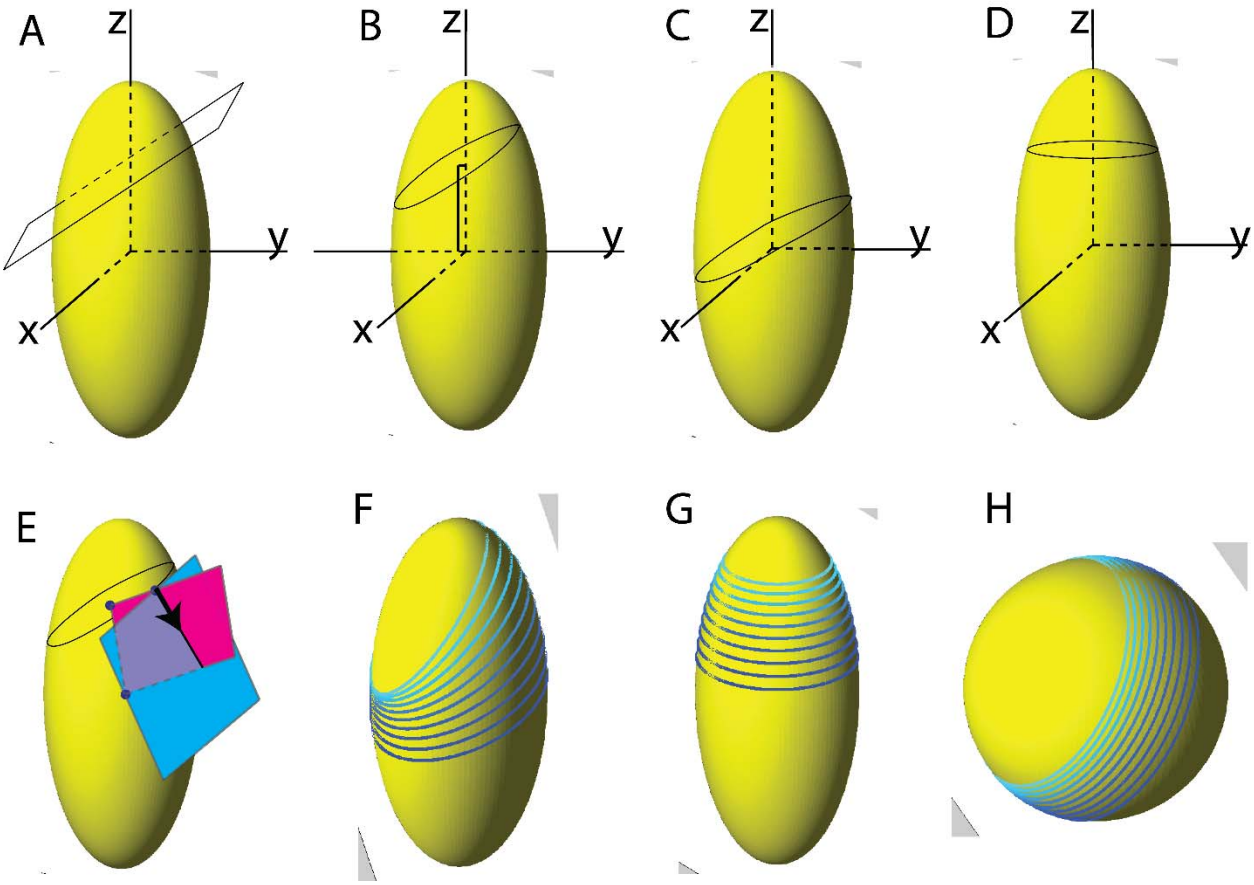

Figure S4: 3D models of CCT. (A) The blastoderm margin can be modeled as a ring obtained by intersecting a plane with the yolk ellipsoid. (B) Any intersection of a plane of positive slope and intercept in the *yz*-plane results in a ring that has a center that lies along the y-axis (x = 0) with a negative y-coordinate (y < 0).e. (C) Any plane that cuts through the origin will have a center at the origin. (D) As predicted, a level plane creates a symmetric ring around the z-axis with a constant center at x = 0 and y = 0. (E) A tangential vector (black vector) to a point on the ellipsoid can be calculated by intersecting the plane tangent to the surface at that point (blue plane) with a plane that is defined by the point on the surface, the center of the ring, and the center of the ellipsoid (pink plane with points indicated by purple dots). (F) In the asymmetric embryo, we see that the 3D evolution of the ring exhibits differential migration as time progresses (indicated by the darkening of the blue lines). (G-H) Control models of the embryo show uniform migration on a symmetric ellipsoid (G) as well as for a spherical yolk (H).

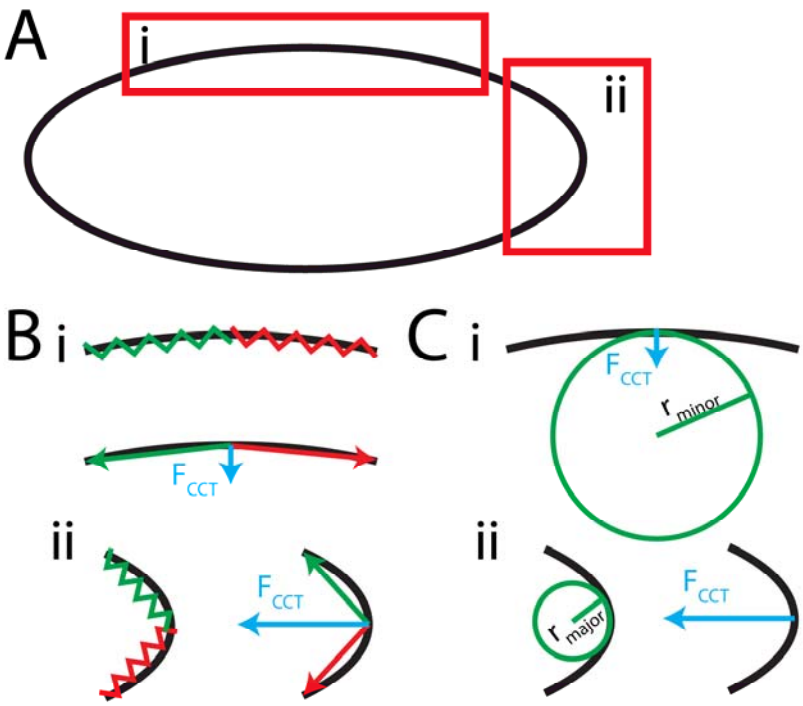

Figure S5: Description of F_{CCT} on an ellipse. (A) In a general ellipse, we will look at the areas corresponding to the minor axis (i) and major axis (ii) and observe the magnitude of F_{CCT} using the spring model and curvature model. (B) Magnitude of F_{CCT} using the spring model. (i) F_{CCT} at the minor axis using the spring model. (*Top*) At the point along the minor axis of the ellipse, the spring pulls equally on the left (green) and right (red) side. (*Bottom*) Most of the force of the springs is projected perpendicularly to the direction of F_{CCT} (green and red) which results in a small total F_{CCT} (blue). (ii) F_{CCT} at the major axis using the spring model. (*left*) At the point along the major axis of the embryo, the spring pulls equally above (green) and below (red) the point. (*right*) Due to the high curvature, the spring forces (green and red) are more directed towards the center of the ring leading to high overall F_{CCT}. (C) Magnitude of F_{CCT} using the curvature model. (i) At the minor axis point, the radius of curvature, as determined by the radius of circle that is tangent to that point (r_{minor}, green), is large. Since F_{CCT} is inversely proportional to r_{minor}, this leads to a small overall F_{CCT}. (ii) At the major axis point, the radius of curvature (r_{major}, *left, green*) is small, F_{CCT} is large. In both the spring and curvature model, F_{CCT} is small at the minor axis and large at the major axis.

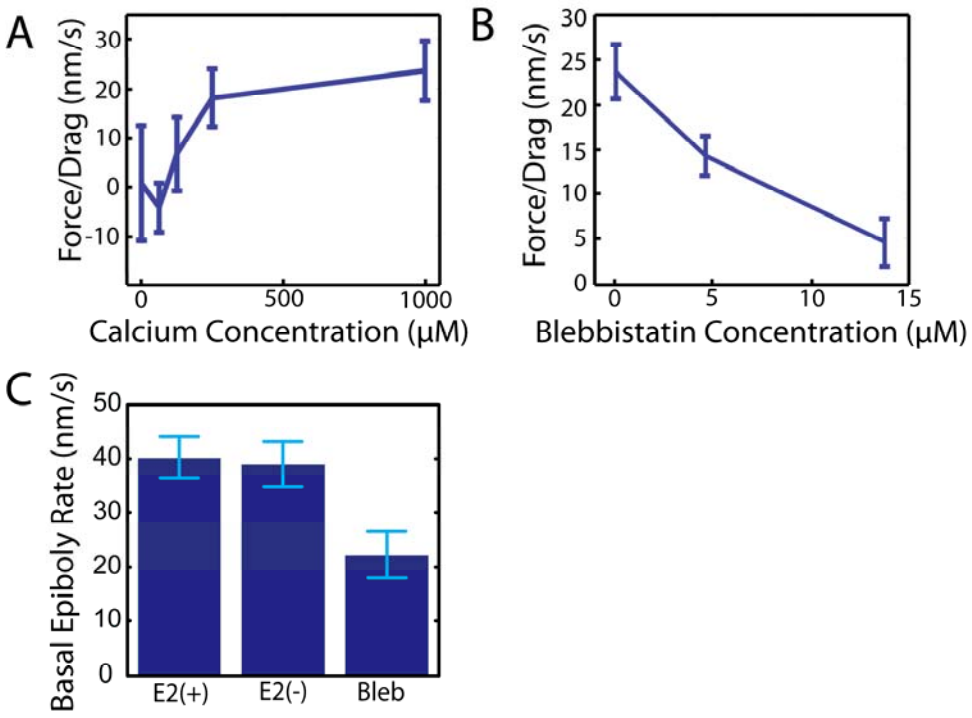

Figure S6: Dose dependence of chemical treatments that affect the basal rate of epiboly. (A) F_{CCT}/c_{Drag} as a function of media Ca^{2+} concentration. (B) F_{CCT}/c_{Drag} as a function of blebbistatin concentration. Both treatments block blastoderm margin reorientation in a dose-dependent manner. (C) Basal rates of epiboly in multiple embryos grown in different conditions were calculated by averaging the rate of the left and right edge of the margin at different time points. The basal epiboly rate is statistically identical for embryos grown in E2 (E2(+)) and in reduced Ca2+ (E2(-); 62.5 μM; $P = 0.70$). However, when blebbistatin is introduced, the basal epiboly rate is decreased significantly. ($P < 0.0001$). The error bars represent standard error.

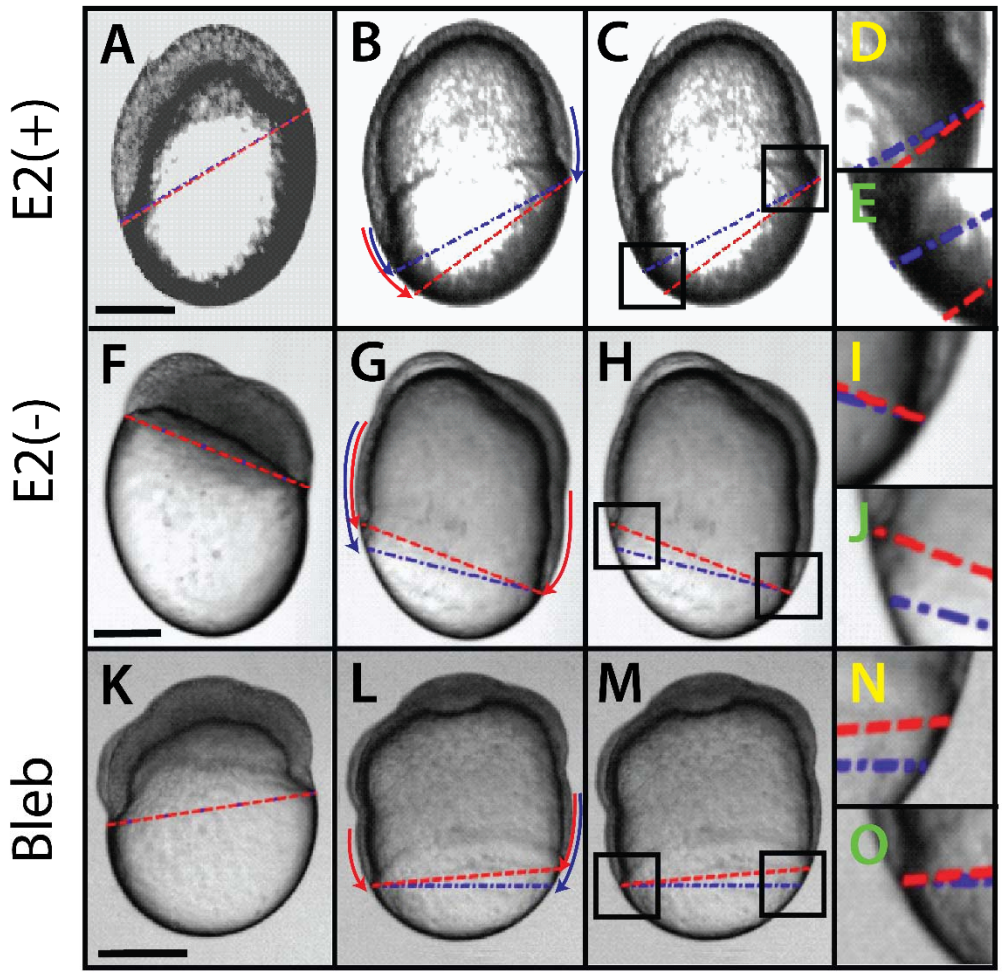

Figure S7: An analytic model recapitulates local variations in blastoderm migration over 3 hours in asymmetric embryos. Blue lines indicate the predicted blastoderm edges using a model that incorporates a CCT force component. Red lines indicate the predicted edges for a model lacking a contribution from CCT. For an embryo grown in normal E2 (E2(+); *top row*, A-E) the model that includes CCT (blue lines) predicts the location of the blastoderm edges whereas a model lacking CCT does not (red lines). Embryos grown in reduced Ca^{2+} (62.5 µM) E2 (E2 (-); *middle row*, F-J) or E2 plus 13.8 µM blebbistatin (Bleb; *bottom row*, K-O) are better predicted by a model that does not incorporate CCT (red lines). (D, I, N) Zoomed in images of the left edge of the blastoderm margin. (E, J, O) Zoomed in images of the right edge of the blastoderm margin. (Scale bar = 250 µm)

Condition	n	Slope (nm/s)	p-value (Slope = 0)	Intercept (nm/s)	p-value (Intercept = 0)
Normal E2 (1mM Ca^{2+}) (E2(+))	16	23±6	0.0001	0.30±1.56	0.84
E2 + 0.25 mM Ca^{2+}	11	18±6	0.003	-1.58±1.42	0.27
E2 + 0.125 mM Ca^{2+}	10	7±7	0.38	-2.10±1.74	0.23
E2 + 0.0625 mM Ca^{2+} (E2(-))	15	-4±5	0.82	4.26±1.50	0.005
E2 + 4.6 μM Blebbistatin	14	18±5	0.001	2.75±1.82	0.13
E2 + 13.8 μM Blebbistatin (Bleb)	11	3±5	0.56	2.22±1.75	0.21

Table 1: Linear fits of Δv vs $\Delta\cos\theta$ in compressed embryos have y-axis intercepts that are close to zero and slope values that vary depending on Ca^{2+} and blebbistatin concentration, suggesting differences in F_{CCT} (cf. Figure 3C, 4B, S2). These results agree with the control case of uncompressed embryos in which uniform blastoderm migration is observed. According to Equation 4, the plot of Δv vs $\Delta\cos\theta$ should have a slope that corresponds to F_{CCT}/c_{Drag} and an intercept that corresponds to $\Delta F_{Tan}/c_{Drag}$. The observation that the intercept is close to 0 in all cases supports the hypothesis that tangential forces are uniform and that ΔF_{Tan} can assumed to be 0.

Movie S1: Related to Figure 2. Movie of a compressed embryo grown in E2 media. Blue lines indicate the predicted edges of the blastoderm margin using a model incorporating F_{CCT}/c_{Drag} value of 28 nm s^{-1}. Red lines indicate the predicted edges of the blastoderm margin using a model without incorporating CCT. Over the course of epiboly, the model that incorporates CCT (blue) better predicts the position of the blastoderm margin.

Movie S2: Related to Figure 3. Movie showing the progression of epiboly on a 3D asymmetric ellipsoid. (Left) At each marginal ring, a uniform tangential force (red) is generated around the ring directed along the tangent of the ellipsoid while a force due to CCT (green) is generated around the ring and points toward its center. (Middle) Due to the uneven contribution of CCT (green), on the left side CCT projects negatively onto the tangent while on the right side CCT projects positively onto the tangent. Combining this with the uniform tangential force results in uneven net tangential forces (Right, maroon). Consequently, the right side of the ring progresses faster than the left side, resulting in reorientation of the ring perpendicular to the long axis of the ellipsoid.

Movie S3: Related to Figure 3. Movie showing the progression of epiboly on a 3D ellipsoid with a symmetric ring (top) and on a sphere (bottom). (Left) CCT (green) produces a uniform force around the ring along with a uniform tangent force (red). Since the ring is symmetric, CCT provides an equal contribution of force to the tangent at each point on the ring resulting in a uniform net tangential force (right, maroon). Consequently, the ring progresses uniformly down both the ellipsoid and the sphere.

Movie S4: Related to Figure 4. Movie showing a compressed embryo grown in reduced Ca^{2+} (62.5 μM) media. Blue lines indicate the predicted edges of epiboly using a model incorporating a F_{CCT}/c_{Drag} value of 28 nm s^{-1}. Red lines indicate the predicted edges of epiboly using a model without incorporating CCT. Over the course of epiboly, the model that lacks CCT (red) better predicts the position of the blastoderm margin edges.

Movie S5: Related to Figure 4. Movie showing a compressed embryo grown in media with 13.8 μM blebbistatin. Blue lines indicate the predicted edges of epiboly using a model that

incorporates a F_{CCT}/c_{Drag} value of 28 nm s^{-1}. Red lines indicate the predicted edges of epiboly using a model without incorporating CCT. Over the course of epiboly, the model that lacks CCT (red) better predicts the position of the blastoderm margin edges.

Movie S6: Related to Figure 5. Movie of a compressed embryo grown in normal E2 (left) and in reduced Ca^{2+} (62.5 μM, right) media over 18.6 hours. In both cases, the embryos develop properly through the conclusion of epiboly.

1. Babb, S. G., and J. A. Marrs. 2004. E-cadherin regulates cell movements and tissue formation in early zebrafish embryos. Dev Dyn 230:263-277.
2. Behrndt, M., G. Salbreux, P. Campinho, R. Hauschild, F. Oswald, J. Roensch, S. W. Grill, and C. P. Heisenberg. 2012. Forces driving epithelial spreading in zebrafish gastrulation. Science 338:257-260.
3. Bonneau, B., N. Popgeorgiev, J. Prudent, and G. Gillet. 2011. Cytoskeleton dynamics in early zebrafish development: A matter of phosphorylation? Bioarchitecture 1:216-220.
4. Manning, M. L., R. A. Foty, M. S. Steinberg, and E. M. Schoetz. 2010. Coaction of intercellular adhesion and cortical tension specifies tissue surface tension. Proc Natl Acad Sci U S A 107:12517-12522.
5. Solnica-Krezel, L., and W. Driever. 1994. Microtubule arrays of the zebrafish yolk cell: organization and function during epiboly. Development 120:2443-2455.
6. Song, S., S. Eckerle, D. Onichtchouk, J. A. Marrs, R. Nitschke, and W. Driever. 2013. Pou5f1-dependent EGF expression controls e-cadherin endocytosis, cell adhesion, and zebrafish epiboly movements. Dev Cell 24:486-501.
7. Strahle, U., and S. Jesuthasan. 1993. Ultraviolet irradiation impairs epiboly in zebrafish embryos: evidence for a microtubule-dependent mechanism of epiboly. Development 119:909-919.
8. Cheng, J. C., A. L. Miller, and S. E. Webb. 2004. Organization and function of microfilaments during late epiboly in zebrafish embryos. Dev Dyn 231:313-323.
9. Holloway, B. A., S. Gomez de la Torre Canny, Y. Ye, D. C. Slusarski, C. M. Freisinger, R. Dosch, M. M. Chou, D. S. Wagner, and M. C. Mullins. 2009. A novel role for MAPKAPK2 in morphogenesis during zebrafish development. PLoS Genet 5:e1000413.